This information accompanies and completes the manuscript titled "*Optimizing sampling strategies in high-resolution paleoclimate records*" submitted for publication in Climate of the Past. The document below contains a guide to the Supplementary Data files accompanying this submission, lists several additional result plots not included in the main submission and ends with some supplementary discussion on the applications of this work in future studies. All supplementary files are also stored in the online open-source database Zenodo (www.doi.org/10.5281/zenodo.3899926).

Overview Supplementary Data

File name	Description
S1: Overview scenarios	Detailed overview of the specifics of all scenarios tested within this study. Lists variability in SST, growth rate, $\delta^{18}O_w$, sampling density, record, length and age model uncertainty along with a short description of what type of natural variability each case is meant to represent/test. An abridged version of this table is included in the main text as **Table 1**.
S2: Texel hourly SST/SSS	Hourly SST and SSS measurements made between 2001 and 2016 at the NIOZ measuring station in the harbor on the south side of Texel island (NW the Netherlands, see case 30, **Fig. 3** in main text), obtained with help from Sonja van Leeuwen and Eric Wagemaakers (pers. comm.; see **Fig. S1**). This dataset was used as a basis for defining variability on the seasonal vs. weather scale, with weather-scale variability being added to the virtual cases (cases 1-29) to more closely approximate natural circumstances. $\delta^{18}O_w$ values are obtained from SSS measurements using the mass balance presented in the main text.
S3: Normality test (R)	Script for testing the normality of "weather" residuals of SST and SSS after subtracting the seasonal cycle through a Kolmogorov-Smirnov test (see **Fig. S1**).
S4: Data overview	Overview of true and reconstructed SST and $\delta^{18}O_w$ data for all reconstruction approaches. Includes calculations of accuracy and precision for all cases, at every sampling density and using all reconstruction approaches. Also includes separate sheets in which the effect of a certain parameter (e.g. sampling density) is isolated, which serve as basis for **Figures 8-11** in the main manuscript.
S5: Generate virtual data (R)	Script used to generate virtual $\delta^{18}O_c$ and Δ_{47} data from SST and SSS curves of all virtual cases. The functions used to generate these "virtual carbonate archives" were compiled in the documented R package ***seasonalclumped*** which is available on the open-source online repository CRAN (de Winter, 2021).
S6: Virtual data overview	Overview of virtual data generated for all cases (1-33) using the script in **S5**. All virtual datasets were also included as internal datasets in the documented R package ***seasonalclumped*** which is available on the open-source online repository CRAN (de Winter, 2021).
S7: Combined data processing routine (R)	Script listing the formulae used to calculate monthly SST and $\delta^{18}O_w$ reconstructions from the virtual data sets provided in **S6**. The functions used to do these reconstructions were compiled in the documented R package ***seasonalclumped*** which is available on the open-source online repository CRAN (de Winter, 2021).
S8: Raw data results and figures	Large folder containing all raw exported datasheets from the script in **S7**, listing all in between steps of the SST and $\delta^{18}O_w$ reconstructions as well as figures comparing the results of all these reconstructions on all cases for every sampling density.

S9: Accuracy and precision table	Color-coded table showing the differences in accuracy and precision of mean annual and seasonal SST and $\delta^{18}O_w$ reconstructions on all cases using the four different reconstruction methods (basis for Figures 6 and 7; see also **Figures XXX and XXX**).
S10: Optimal sample size results	Overview of the median optimal sample sizes required for successful separation of summer and winter sample groups for seasonality reconstructions in all cases through the optimization approach.

Supplementary Figures

Below we list several supplementary figures illustrating additional aspects of the results of this study which were not shown in the figures in the main text.

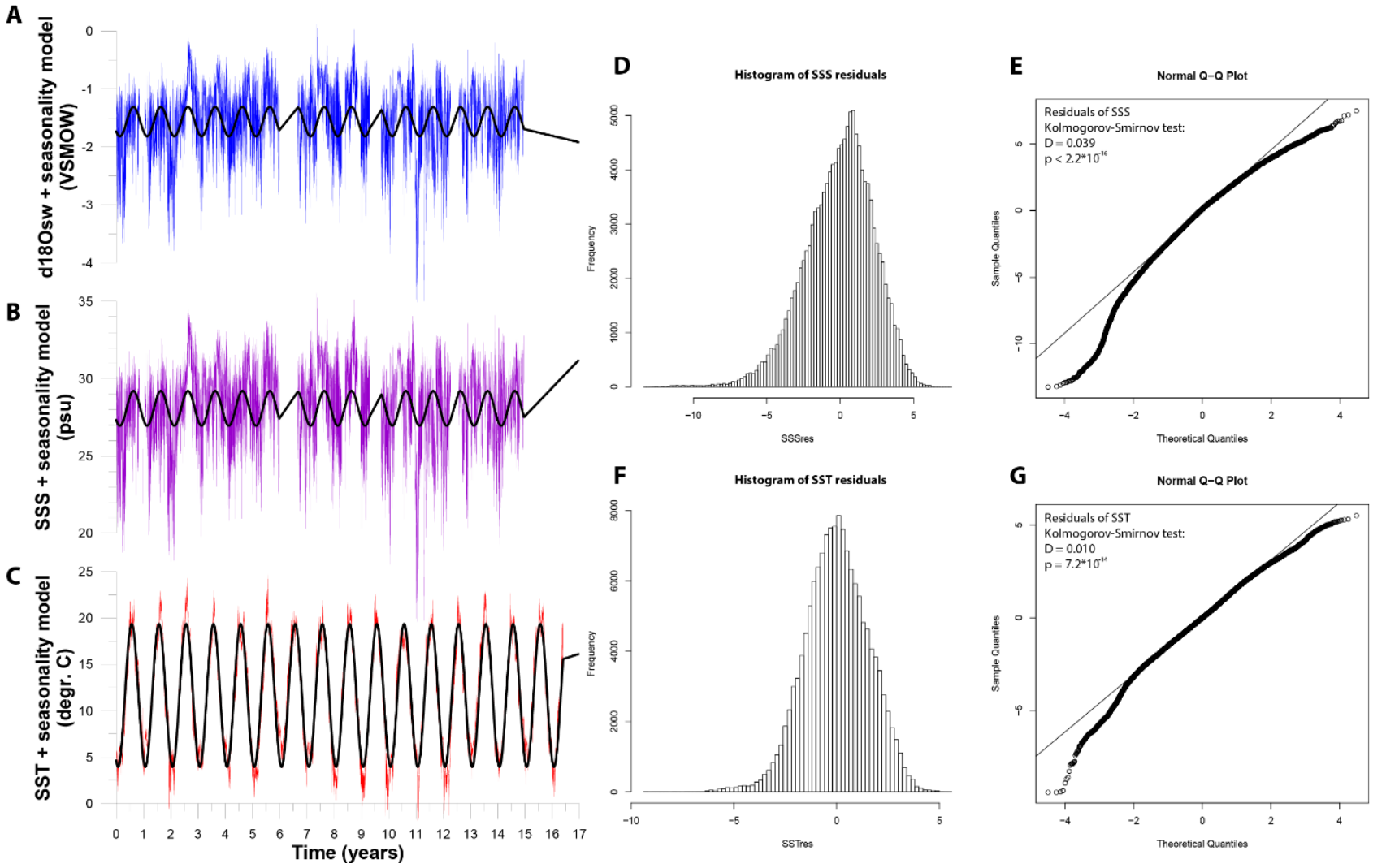

Figure S1: Seasonality and "weather-scale" variability in measured SST and SSS and modelled $\delta^{18}O_w$ values from the Texel locality (case 30; see **S2**). With **A** showing hourly $\delta^{18}O_w$ variability (in blue) over time (years 2001-2016) modelled from hourly SSS measurements (**B**; in purple) with the

black line showing a sinusoidal fit through the data to represent the seasonal component. **C** shows the same for hourly SST measurements (in red). The histograms and Q-Q plots in **D-G** show the distribution of the residuals in SSS (**D** and **E**) and SST (**F** and **G**) obtained by subtracting the seasonality (black lines in **A-C**) from the SST and SSS records. Note that the Kolmogorov-Smirnov test (**E** and **G**) demonstrates that both SST and SSS residuals ("weather-scale" variability) are not normally distributed ($P << 0.05$).

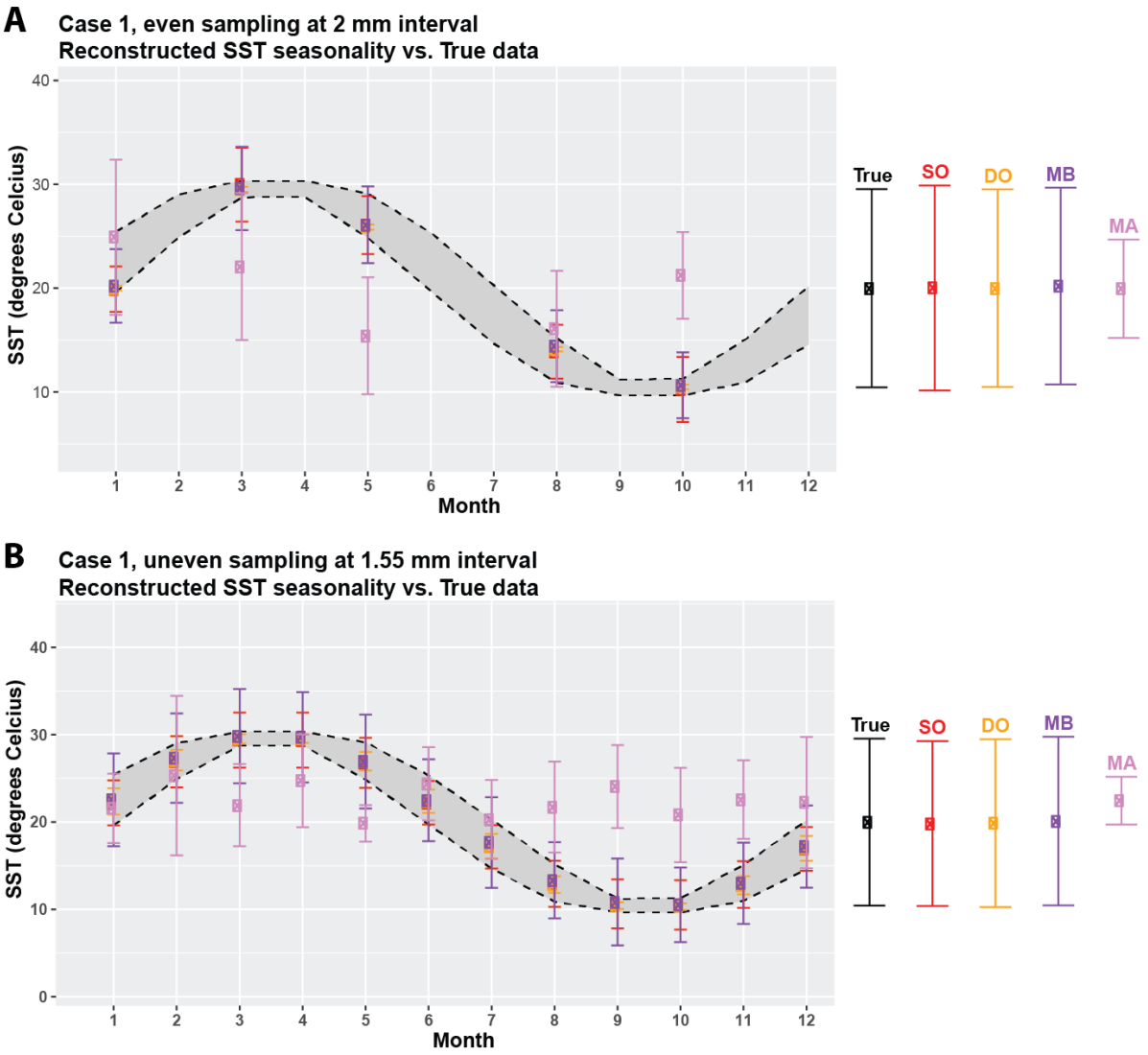

Fig. S2: Comparison of the same reconstructions using the 4 different approaches on case 1 using (**A**) an even sampling interval of 2 mm (an integer fraction of the 10 mm/yr growth rate) or (**B**) and uneven sampling interval of 1.55 mm (not an integer fraction of the growth rate). Note how even sampling intervals cause some months to be oversampled while some other months never contain samples. Consequently, no reconstruction can be done for these months and the resulting seasonal and mean annual reconstructions run the risk of being biased. On the contrary, uneven sampling intervals (**B**) result in different months being sampled in different growth years and yield equal sample distributions across the months, leading to more accurate mean annual and seasonal SST and $\delta^{18}O_w$ reconstructions from monthly data. Bars on the right-hand side show mean annual and seasonality SST reconstructions in both cases.

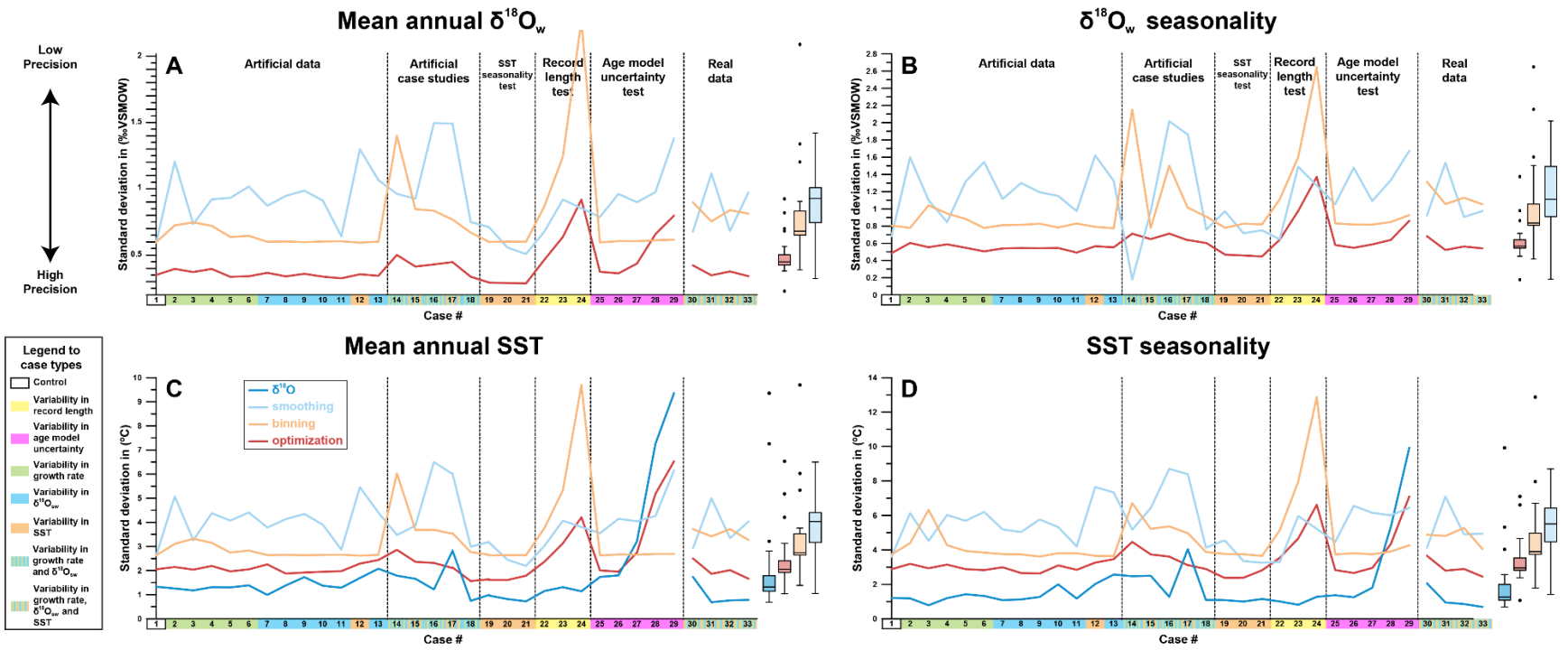

Fig. S3: *Overview of precision (one standard deviation) of reconstructions of mean annual* $\delta^{18}O_w$ $\delta^{18}O_{sw}$ (***A***), *seasonal range in* $\delta^{18}O_w$ $\delta^{18}O_{sw}$ (***B***), *mean annual SST (**C**) and seasonal range in SST (**D**), with higher values indicating lower precision (higher precision errors) based on average sampling resolution (sampling interval of 0.45 mm). The horizontal axis displays the different cases, color coded by their difference from the control case (case 1; see legend on the left-hand side). Colored lines indicate the different data treatment approaches. Box-whisker plots to the right show medians and distributions of precision on all cases using different reconstruction approaches (outliers are identified as black dots based on 2x interquartile distance).

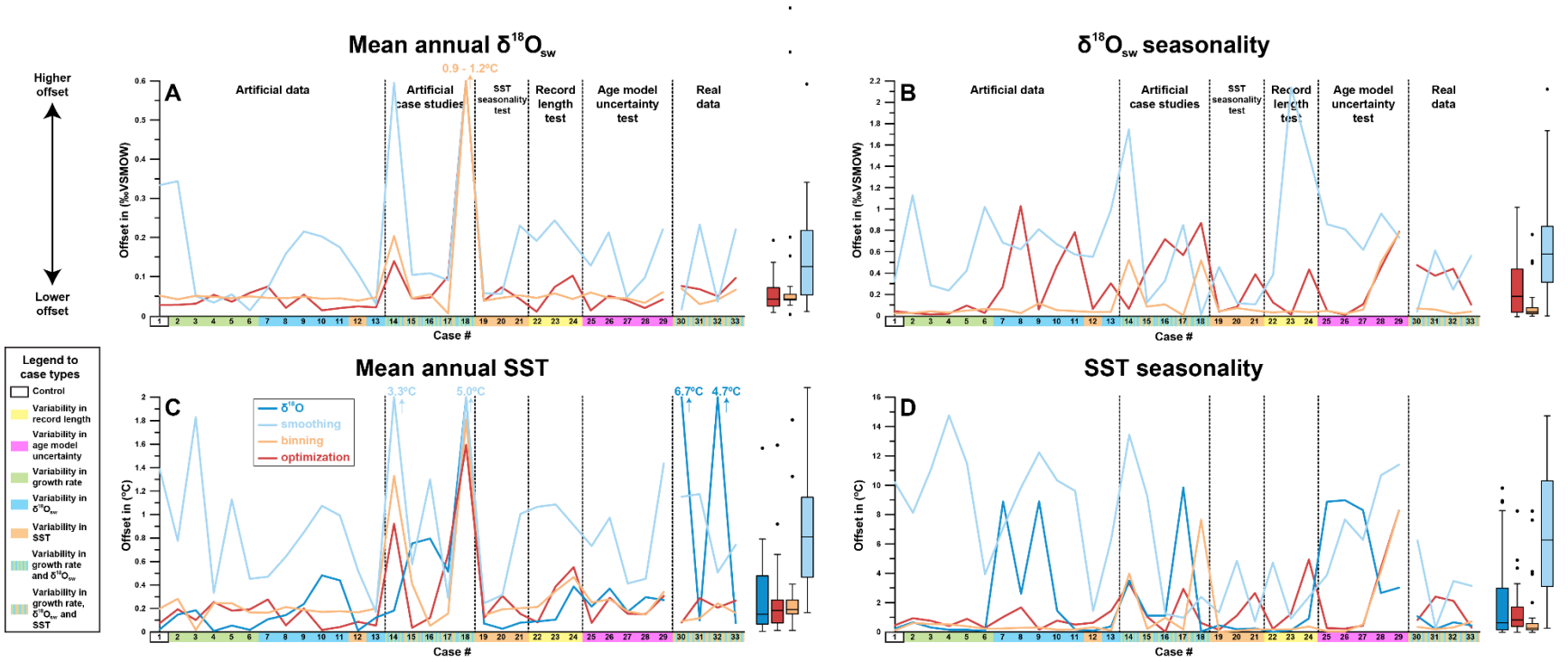

Fig. S4*: Overview of accuracy (absolute difference between reconstruction and "true" value) of reconstructions of mean annual $\delta^{18}O_w$ (**A**), seasonal range in $\delta^{18}O_w$ (**B**), mean annual SST (**C**) and seasonal range in SST (**D**), with higher values indicating lower accuracy (higher offset with "true" value) based on average sampling resolution (sampling interval of 0.45 mm). The horizontal axis displays the different cases, color coded by their difference from the control case (case 1; see legend on the left-hand side). Colored lines indicate the different data treatment approaches. Box-whisker plots to the right show medians and distributions of accuracy on all cases using different reconstruction approaches (outliers are identified as black dots based on 2x interquartile distance).*

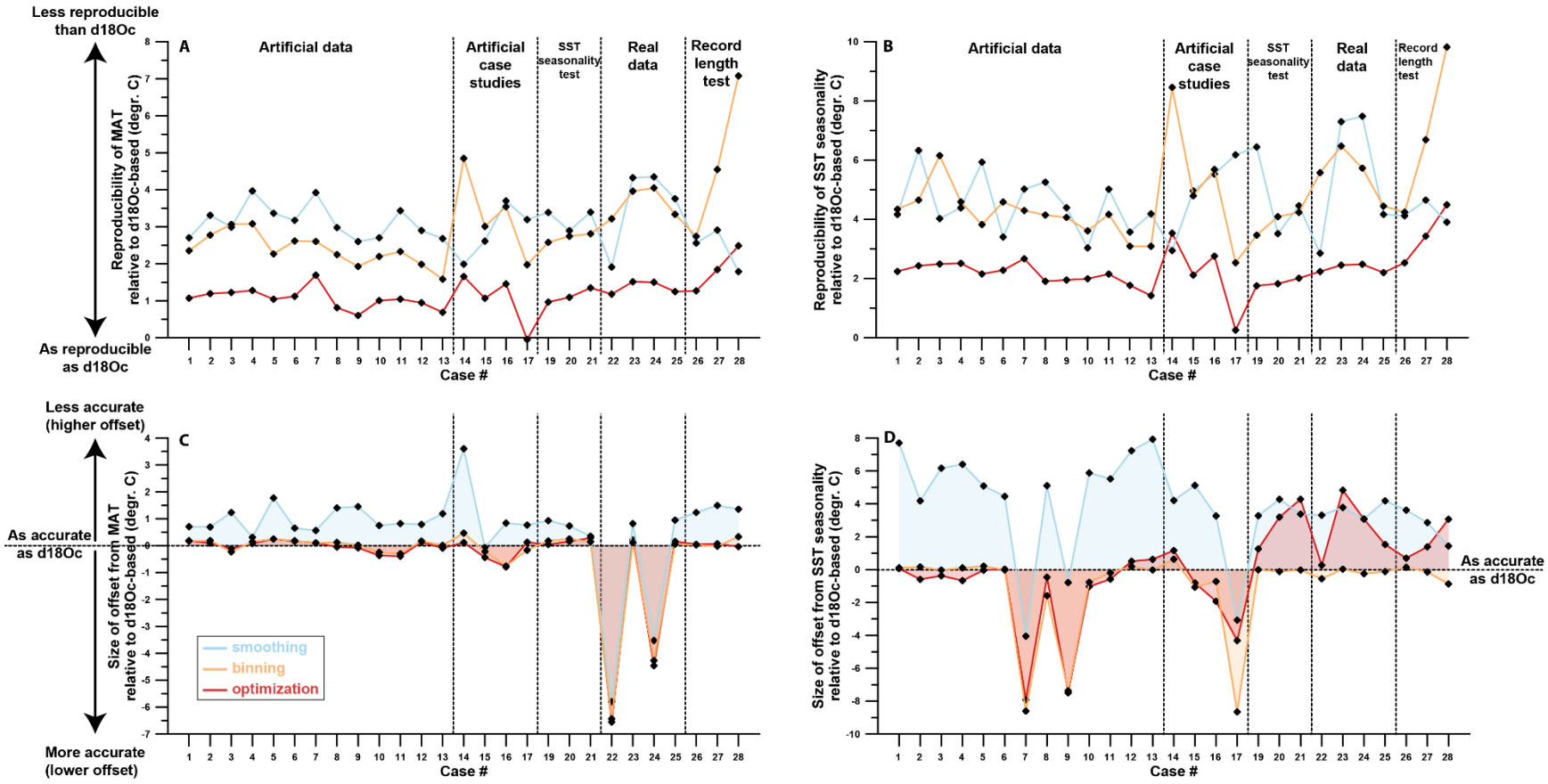

Fig. S5*: Comparison of the precision (MAT:* ***A*** *and SST seasonality:* ***B****) and accuracy (MAT:* ***C*** *and SST seasonality:* ***D****) of the clumped isotope reconstruction approaches (smoothing, binning and optimization) with the* $\delta^{18}O_c$*-based reconstructions (which do not require sample combination). In all figures, higher values (directed upwards) represent less precise/accurate results, with "0" representing equal accurate/precise results as the* $\delta^{18}O_c$*-based reconstructions. Only fully artificial cases are shown and case 18 is omitted.*

.

Supplementary discussion: Implications for other sample size problems

While the discussion above focuses on optimizing approaches for combining samples for clumped isotope analyses in paleoseasonality reconstructions, the problem of combining samples to lower uncertainty and isolate variation in datasets is very common (e.g. Zhang et al., 2004; Merz and Thieken, 2005; Tsukakoshi, 2011). Therefore, the approaches outlined and tested in this study have applications beyond paleoseasonality reconstructions. Below, we briefly highlight four examples of problems that could benefit from applying similar approaches for lowering the uncertainty of estimates of target variables or reducing the number of analyses required to meet analytical requirements.

Tooth bioapatite

Enamel from vertebrate teeth constitute a useful archive for paleoenvironmental and paleoecological change in the terrestrial realm, complementing the carbonate records discussed in this work (e.g. Luz and Kolodny, 1985; Fricke et al., 1996; Balasse, 2002; Van Dam and Reichart, 2009; de Winter et al., 2016). However, the tooth bioapatite archive suffers from similar limitations of sample size and resolution as carbonate archives when it comes to reconstructing high-resolution variability (see discussion in Passey and Cerling, 2002 and Kohn, 2004). Oxygen and carbon isotopes of carbonate and phosphate in tooth enamel contain valuable information about the animal's life cycle and environment (e.g. Fricke et al., 1996; Balasse et al., 2002; Van Dam and Reichart, 2009). However, structurally bound carbonate constitutes a mere 2-5% of tooth enamel (LeGeros et al., 1986), and enamel samples need to be pretreated to remove labile components, so analyses of $\delta^{18}O$ in these archives require comparatively large sample sizes (0.5-1 mg; Fricke et al., 1998; Balasse, 2002; Pellegrini and Snoeck, 2016). Phosphate-bound $\delta^{18}O$ is less susceptible to diagenesis, but requires a more complicated procedure to analyze, resulting in similar sample size limitations (Joachimski et al., 2004; Lecuyer et al., 2007). Most applications of isotope profiles from teeth rely on precise determination of both the phase and amplitude of the seasonal cycle, and therefore suffer from the same complications as isotope records in carbonate archives (e.g. Balasse et al., 2002; Straight et al., 2004). The **binning** and **optimization** approaches discussed here could help reduce uncertainty and provide a basis for better comparison of seasonal profiles in tooth enamel.

Cyclostratigraphy

Within the field of cyclostratigraphy, a multitude of stratigraphical approaches have been developed for signal processing, with the aim to use regular orbital cycles expressed in stratigraphic time series as tools for dating rock sequences (e.g. Paillard et al., 1996; Meyers, 2014; Sinnesael et al., 2016). However, the focus on timing has caused many methods for extracting the climatic impact of these orbital cycles from stratigraphic records (e.g. bandpass filtering; Hilgen, 1991) to remain qualitative. This is unfortunate, because the magnitude of the effect of this cyclicity on climate and environmental change is of major interest in paleoclimatology studies (e.g. Berger, 1992; Shackleton, 2000; Zachos et al., 2001; Lourens et al., 2005; De Vleeschouwer et al., 2017a). The problem of quantitatively extracting the impact of orbital cycles is very similar to the problem of paleoseasonality reconstructions central to this study, and the same approaches can therefore be used in the orbital time domain. The time **binning** approach is probably most robust for this purpose, since cyclostratigraphic records are often longer (record length >> period of the cycle) and sampling resolutions (samples/cycle) are often lower than in seasonal records (see above; e.g. De Vleeschouwer et al., 2017b). Quantitative analyses of the contribution of orbital cyclicity to rhythmic changes in paleoclimate can help separate variability in records caused by external forcing from autocyclic behavior or (positive or negative) feedback of the climate system itself (Lourens et al., 2010; Noorbergen et al., 2017; Nohl et al., 2018).

Strontium isotope dating

Another type of analysis that could benefit from smart combination of measurement results is strontium isotope dating. The strontium isotope composition ($^{87}Sr/^{86}Sr$) of the ocean has evolved over time, and the isotopic composition of marine carbonates can therefore be used to estimate the age of the sample by comparing it with a composite strontium isotope curve (Elderfield, 1986; McArthur et al., 2012). In time intervals where the global marine strontium isotope curve is steep, strontium isotope dating ranks among the most precise methods for absolute dating in stratigraphy (Wagreich et al., 2012). However, accurate dating based on the strontium isotope curve requires propagation of errors on the composite curve and the sample. Doing so results in asymmetric errors due to the non-linear character of the strontium isotope curve, which require complex error propagation (see Barlow, 2003; 2004; Wan et al., 2019). The state-of-the-art uncertainty of individual strontium isotope analyses ranges between 2-10 ppm (1 standard deviation;

Yobregat et al., 2017), which translates to an age uncertainty of 100-200 kyr, (1 standard deviation) depending strongly on the slope of the global strontium isotope curve at the time interval under study. Combining multiple strontium isotope analyses from the same stratigraphic unit can reduce the uncertainty on these composite ages (Korte and Ullmann, 2016; de Winter et al., 2020b), allowing the dating method to be combined with cyclostratigraphy to produce for orbital scale age models (see above). In stratigraphy studies that use this dating method, the need arises to compromise between the resolution of the age model and the precision and accuracy of dating, analogous to the tradeoff that occurs when combining Δ_{47} analyses for paleoseasonality reconstructions outlined in this study. In this case, the **smoothing** approach with a dynamic moving window discussed in this study is likely the best candidate for combining data to improve these age models. Such an approach can be seen as a more flexible adaptation of the Δ_{47}-based approach for SST reconstruction outlined in Rodríguez-Sanz et al. (2017) that provides the flexibility to adapt the sample window depending on the available data and the slope of the global strontium curve. At the same time, the shape of the global composite strontium isotope curve itself can be refined by using a similar protocol on well-dated samples. The approaches discussed in this study are more adaptable to changes in sampling density over time and can in theory achieve higher precision than the LOWESS fit approach currently employed for constructing the global composite (McArthur et al., 2012). Similarly, techniques for compromising between sampling resolution and accuracy and precision can be applied to improve other dating methods based on matching curves such as radiocarbon dating (Ramsay and Lee, 2013), carbon isotope stratigraphy (Salzman and Thomas, 2012) and dendrochronology (Cook and Kairiukstis, 2013).

Sub-seasonal variability

Ultra-high-resolution records from fast-growing archives (e.g. mollusks) are an emerging phenomenon in the field of high-resolution paleoclimatology (e.g. Sano et al., 2012; Warter and Müller, 2017, de Winter et al., 2020a). The emergence of such records allows new information to be obtained about the daily cycle (Warter et al., 2018; de Winter et al., 2020a) and extreme weather events (Yan et al., 2020) in the past, potentially bridging the gap between weather and climate reconstructions. The sampling resolution required to resolve variability at such a fine temporal scale warrants an even more careful consideration of the

tradeoff between sample size, sampling resolution and analytical uncertainty than the paleoseasonality examples considered here. If quantitative estimates of insolation, temperature and the frequency of extreme weather events are to be reconstructed from these novel records, a compromise will need to be found between analytical uncertainty and the temporal resolution of measurements (Sano et al., 2012; de Winter et al., 2020a; Yan et al., 2020). Applying the temporal (e.g. hourly) binning method (**binning**) discussed here on long, (sub-)daily resolved records could yield more accurate and precise records of ultra-high-resolution variability, given its reliability in extracting accurate cycle amplitude (e.g. seasonality) from long, less densely sampled records (see discussion in main text). Fast-growing bivalve and gastropod shells have already been marked as promising archives for such variability, while other fast-growing archives such as *Acropora* corals remain to be explored (Bak et al., 2009; Strauss et al., 2014; de Winter et al., 2020c). It must be noted that models for the timing of carbonate deposition in accretionary carbonate archives at the sub-daily scale are highly uncertain and that this may complicate the use of the **binning** approach (see discussion in main text), in which case **optimization** may be more appropriate.

Event stratigraphy

Accurate and precise temperature reconstructions of short-lived (10-100 kyr) episodes of climate change present a problem comparable to resolving seasonality in paleoclimate archives. Examples of such events include the Mesozoic ocean anoxic events (Hesselbo et al., 2000; Jenkyns, 2010), early Paleogene hyperthermals (Stap et al., 2010; Lauretano et al., 2015, 2018) and stepwise climate perturbations such as the Eocene-Oligocene transition (Dupont-Nivet et al., 2007; Lear et al., 2008) studied in deep-sea records. Currently, reconstructions of temperature variability in the deep-sea during such events are based on benthic foraminiferal $\delta^{18}O_c$ (e.g. Erbacher et al., 2001; Lui et al., 2009; Stap et al., 2010; Lauretano et al., 2015, 2018), but may not be reliable due to assumptions made on $\delta^{18}O_{sw}$. Deep-sea sedimentary environments are generally characterized by low sedimentation rates (~1 cm/kyr) as well as low abundance and small size of microfossils (e.g. foraminifera) which serve as archives of past marine conditions (e.g. Stap et al., 2010; Jennions et al., 2015). This limits the number of aliquots that can be obtained for Δ_{47} and other analyses through these climate events. In these studies, a **smoothing** approach would probably underestimate the 'true' amplitude of temperature or geochemical change. With sufficient record length and

perhaps by combining multiple events, **binning** or **optimization** based on proxy data would be the most accurate and precise approach to resolve transient temperature change in the deep-sea during the geological past.

REFERENCES

Bak, R. P., Nieuwland, G. and Meesters, E. H.: Coral growth rates revisited after 31 years: what is causing lower extension rates in Acropora palmata?, Bulletin of Marine Science, 84(3), 287–294, 2009.

Balasse, M.: Reconstructing dietary and environmental history from enamel isotopic analysis: time resolution of intra-tooth sequential sampling, International Journal of Osteoarchaeology, 12(3), 155–165, 2002.

Balasse, M., Ambrose, S. H., Smith, A. B. and Price, T. D.: The Seasonal Mobility Model for Prehistoric Herders in the South-western Cape of South Africa Assessed by Isotopic Analysis of Sheep Tooth Enamel, Journal of Archaeological Science, 29(9), 917–932, https://doi.org/10.1006/jasc.2001.0787, 2002.

Barlow, R.: Asymmetric systematic errors, arXiv preprint physics/0306138, 2003.

Barlow, R.: Asymmetric errors, arXiv preprint physics/0401042, 2004.

Berger, A. L.: Astronomical theory of paleoclimates and the last glacial-interglacial cycle, Quaternary Science Reviews, 11(5), 571–581, 1992.

Cook, E. R. and Kairiukstis, L. A.: Methods of dendrochronology: applications in the environmental sciences, Springer Science & Business Media., 2013.

van Dam, J. A. and Reichart, G. J.: Oxygen and carbon isotope signatures in late Neogene horse teeth from Spain and application as temperature and seasonality proxies, Palaeogeography, Palaeoclimatology, Palaeoecology, 274(1–2), 64–81, https://doi.org/10.1016/j.palaeo.2008.12.022, 2009.

De Vleeschouwer, D., Vahlenkamp, M., Crucifix, M. and Pälike, H.: Alternating Southern and Northern Hemisphere climate response to astronomical forcing during the past 35 my, Geology, 45(4), 375–378, 2017a.

De Vleeschouwer, D., Da Silva, A.-C., Sinnesael, M., Chen, D., Day, J. E., Whalen, M. T., Guo, Z. and Claeys, P.: Timing and pacing of the Late Devonian mass extinction event regulated by eccentricity and obliquity, Nature Communications, 8(1), 1–11, https://doi.org/10.1038/s41467-017-02407-1, 2017b.

Dupont-Nivet, G., Krijgsman, W., Langereis, C. G., Abels, H. A., Dai, S. and Fang, X.: Tibetan plateau aridification linked to global cooling at the Eocene–Oligocene transition, Nature, 445(7128), 635–638, 2007.

Elderfield, H.: Strontium isotope stratigraphy, Palaeogeography, palaeoclimatology, palaeoecology, 57(1), 71–90, 1986.

Erbacher, J., Huber, B. T., Norris, R. D. and Markey, M.: Increased thermohaline stratification as a possible cause for an ocean anoxic event in the Cretaceous period, Nature, 409(6818), 325–327, https://doi.org/10.1038/35053041, 2001.

Fricke, H. C., Clyde, W. C. and O'Neil, J. R.: Intra-tooth variations in δ18O (PO4) of mammalian tooth enamel as a record of seasonal variations in continental climate variables, Geochimica et Cosmochimica Acta, 62(11), 1839–1850, 1998.

Hesselbo, S. P., Gröcke, D. R., Jenkyns, H. C., Bjerrum, C. J., Farrimond, P., Morgans Bell, H. S. and Green, O. R.: Massive dissociation of gas hydrate during a Jurassic oceanic anoxic event, Nature, 406(6794), 392–395, https://doi.org/10.1038/35019044, 2000.

Hilgen, F. J.: Astronomical calibration of Gauss to Matuyama sapropels in the Mediterranean and implication for the Geomagnetic Polarity Time Scale, Earth and Planetary Science Letters, 104(2–4), 226–244, https://doi.org/10.1016/0012-821X(91)90206-W, 1991.

Jenkyns, H. C.: Geochemistry of oceanic anoxic events, Geochemistry, Geophysics, Geosystems, 11(3), https://doi.org/10.1029/2009GC002788, 2010.

Jennions, S. M., Thomas, E., Schmidt, D. N., Lunt, D. and Ridgwell, A.: Changes in benthic ecosystems and ocean circulation in the Southeast Atlantic across Eocene Thermal Maximum 2, Paleoceanography, 30(8), 1059–1077, 2015.

Joachimski, M. M., van Geldern, R., Breisig, S., Buggisch, W. and Day, J.: Oxygen isotope evolution of biogenic calcite and apatite during the Middle and Late Devonian, International Journal of Earth Sciences, 93(4), 542–553, https://doi.org/10.1007/s00531-004-0405-8, 2004.

Kohn, M. J.: Comment: tooth enamel mineralization in ungulates: implications for recovering a primary isotopic time-series, by BH Passey and TE Cerling (2002), Geochimica et Cosmochimica Acta, 68(2), 403–405, 2004.

Korte, C. and Ullmann, C. V.: Permian strontium isotope stratigraphy, Geological Society, London, Special Publications, 450(1), 105–118, https://doi.org/10.1144/SP450.5, 2018.

Lauretano, V., Littler, K., Polling, M., Zachos, J. C. and Lourens, L. J.: Frequency, magnitude and character of hyperthermal events at the onset of the Early Eocene Climatic Optimum, Climate of the Past, 11(10), 1313–1324, 2015.

Lauretano, V., Zachos, J. C. and Lourens, L. J.: Orbitally Paced Carbon and Deep-Sea Temperature Changes at the Peak of the Early Eocene Climatic Optimum, Paleoceanography and Paleoclimatology, 33(10), 1050–1065, https://doi.org/10.1029/2018PA003422, 2018.

Lear, C. H., Bailey, T. R., Pearson, P. N., Coxall, H. K. and Rosenthal, Y.: Cooling and ice growth across the Eocene-Oligocene transition, Geology, 36(3), 251–254, 2008.

Lecuyer, C., Fourel, F., Martineau, F., Amiot, R., Bernard, A., Daux, V., Escarguel, G. and Morrison, J.: High-precision determination of 18O/16O ratios of silver phosphate by EA-pyrolysis-IRMS continuous flow technique, Journal of Mass Spectrometry, 42(1), 36–41, 2007.

LeGeros, R., Balmain, N. and Bonel, G.: Structure and composition of the mineral phase of periosteal bone, Journal of chemical research. Synopses, (1), 8–9, 1986.

Liu, Z., Pagani, M., Zinniker, D., DeConto, R., Huber, M., Brinkhuis, H., Shah, S. R., Leckie, R. M. and Pearson, A.: Global cooling during the Eocene-Oligocene climate transition, Science, 323(5918), 1187–1190, 2009.

Lourens, L. J., Sluijs, A., Kroon, D., Zachos, J. C., Thomas, E., Röhl, U., Bowles, J. and Raffi, I.: Astronomical pacing of late Palaeocene to early Eocene global warming events, Nature, 435(7045), 1083–1087, https://doi.org/10.1038/nature03814, 2005.

Luz, B. and Kolodny, Y.: Oxygen isotope variations in phosphate of biogenic apatites, IV. Mammal teeth and bones, Earth and Planetary Science Letters, 75(1), 29–36, 1985.

McArthur, J. M., Howarth, R. J. and Shields, G. A.: Strontium isotope stratigraphy, The geologic time scale, 1, 127–144, 2012.

Merz, B. and Thieken, A. H.: Separating natural and epistemic uncertainty in flood frequency analysis, Journal of Hydrology, 309(1–4), 114–132, 2005.

Meyers, S. R.: Astrochron: An R package for astrochronology, http://cran.r-project.org/package=astrochron. http://scholar.google.com/scholar?cluster=14876361610707754388&hl=en&oi=scholarr, last access: 30 May 2017, 2014.

Nohl, T., Jarochowska, E. and Munnecke, A.: Revealing the genesis of limestone-marl alternations: a taphonomic approach, Palaios, 34(1), 15–31, 2018.

Noorbergen, L. J., Abels, H. A., Hilgen, F. J., Robson, B. E., Jong, E. de, Dekkers, M. J., Krijgsman, W., Smit, J., Collinson, M. E. and Kuiper, K. F.: Conceptual models for short-eccentricity-scale climate control on peat formation in a lower Palaeocene fluvial system, north-eastern Montana (USA), Sedimentology, 65(3), 775–808, https://doi.org/10.1111/sed.12405, 2018.

Paillard, D., Labeyrie, L. D. and Yiou, P.: AnalySeries 1.0: a Macintosh software for the analysis of geophysical time-series, Eos, 77, 379, 1996.

Passey, B. H. and Cerling, T. E.: Tooth enamel mineralization in ungulates: implications for recovering a primary isotopic time-series, Geochimica et Cosmochimica Acta, 66(18), 3225–3234, 2002.

Pellegrini, M. and Snoeck, C.: Comparing bioapatite carbonate pre-treatments for isotopic measurements: Part 2—Impact on carbon and oxygen isotope compositions, Chemical Geology, 420, 88–96, 2016.

Ramsey, C. B. and Lee, S.: Recent and Planned Developments of the Program OxCal, Radiocarbon, 55(2), 720–730, https://doi.org/10.1017/S0033822200057878, 2013.

Rodríguez-Sanz, L., Bernasconi, S. M., Marino, G., Heslop, D., Müller, I. A., Fernandez, A., Grant, K. M. and Rohling, E. J.: Penultimate deglacial warming across the Mediterranean Sea revealed by clumped isotopes in foraminifera, Scientific Reports, 7(1), 1–11, https://doi.org/10.1038/s41598-017-16528-6, 2017.

Saltzman, M. R. and Thomas, E.: Carbon isotope stratigraphy, The geologic time scale, 1, 207–232, 2012.

Sano, Y., Kobayashi, S., Shirai, K., Takahata, N., Matsumoto, K., Watanabe, T., Sowa, K. and Iwai, K.: Past daily light cycle recorded in the strontium/calcium ratios of giant clam shells, Nature Communications, 3, 761, 2012.

Shackleton, N. J.: The 100,000-Year Ice-Age Cycle Identified and Found to Lag Temperature, Carbon Dioxide, and Orbital Eccentricity, Science, 289(5486), 1897–1902, https://doi.org/10.1126/science.289.5486.1897, 2000.

Sinnesael, M., Zivanovic, M., Vleeschouwer, D. D., Claeys, P. and Schoukens, J.: Astronomical component estimation (ACE v. 1) by time-variant sinusoidal modeling, Geoscientific Model Development, 9, 3517–3531, 2016, 2016.

Stap, L., Lourens, L. J., Thomas, E., Sluijs, A., Bohaty, S. and Zachos, J. C.: High-resolution deep-sea carbon and oxygen isotope records of Eocene Thermal Maximum 2 and H2, Geology, 38(7), 607–610, 2010.

Straight, W. H., Barrick, R. E. and Eberth, D. A.: Reflections of surface water, seasonality and climate in stable oxygen isotopes from tyrannosaurid tooth enamel, Palaeogeography, Palaeoclimatology, Palaeoecology, 206(3), 239–256, https://doi.org/10.1016/j.palaeo.2004.01.006, 2004.

Strauss, J., Oleinik, A. and Swart, P.: Stable isotope profiles from subtropical marine gastropods of the family Fasciolariidae: growth histories and relationships to local environmental conditions, Mar Biol, 161(7), 1593–1602, https://doi.org/10.1007/s00227-014-2443-5, 2014.

Tsukakoshi, Y.: Sampling variability and uncertainty in total diet studies, Analyst, 136(3), 533–539, https://doi.org/10.1039/C0AN00397B, 2011.

Wagreich, M., Hohenegger, J. and Neuhuber, S.: Nannofossil biostratigraphy, strontium and carbon isotope stratigraphy, cyclostratigraphy and an astronomically calibrated duration of the Late Campanian Radotruncana calcarata Zone, Cretaceous Research, 38, 80–96, 2012.

Wan, R., Liu, W., McArthur, J. M. and Wang, Z.: Sr-isotope chronology of carbonate rocks: Quantifying the uncertainty of inversion, in Stratigraphy & Timescales, vol. 4, pp. 35–72, Elsevier, https://doi.org/10.1016/bs.sats.2019.08.003, , 2019.

Warter, V. and Müller, W.: Daily growth and tidal rhythms in Miocene and modern giant clams revealed via ultra-high resolution LA-ICPMS analysis—A novel methodological approach towards improved sclerochemistry, Palaeogeography, Palaeoclimatology, Palaeoecology, 465, 362–375, 2017.

de Winter, N. J.: seasonalclumped: Toolbox for Clumped Isotope Seasonality Reconstructions. https://CRAN.R-project.org/package=seasonalclumped, last access: 4 February 2021, 2021.

de Winter, N. J., Snoeck, C. and Claeys, P.: Seasonal Cyclicity in Trace Elements and Stable Isotopes of Modern Horse Enamel, PloS one, 11(11), e0166678, 2016.

de Winter, N. J., Ullmann, C. V., Sørensen, A. M., Thibault, N., Goderis, S., Van Malderen, S. J. M., Snoeck, C., Goolaerts, S., Vanhaecke, F. and Claeys, P.: Shell chemistry of the boreal Campanian bivalve <i>Rastellum diluvianum</i> (Linnaeus, 1767) reveals temperature seasonality, growth rates and life cycle of an extinct Cretaceous oyster, Biogeosciences, 17(11), 2897–2922, https://doi.org/10.5194/bg-17-2897-2020, 2020a.

de Winter, N. J., Goderis, S., Malderen, S. J. M. V., Sinnesael, M., Vansteenberge, S., Snoeck, C., Belza, J., Vanhaecke, F. and Claeys, P.: Subdaily-Scale Chemical Variability in a Torreites Sanchezi Rudist Shell: Implications for Rudist Paleobiology and the Cretaceous Day-Night Cycle, Paleoceanography and Paleoclimatology, 35(2), e2019PA003723, https://doi.org/10.1029/2019PA003723, 2020b.

de Winter, N. J., Vellekoop, J., Clark, A. J., Stassen, P., Speijer, R. P. and Claeys, P.: The giant marine gastropod Campanile giganteum (Lamarck, 1804) as a high-resolution archive of seasonality in the Eocene greenhouse world, Geochemistry, Geophysics, Geosystems, 21(n/a), e2019GC008794, https://doi.org/10.1029/2019GC008794, 2020c.

Yan, H., Liu, C., An, Z., Yang, W., Yang, Y., Huang, P., Qiu, S., Zhou, P., Zhao, N. and Fei, H.: Extreme weather events recorded by daily to hourly resolution biogeochemical proxies of marine giant clam shells, Proceedings of the National Academy of Sciences, 2020.

Yobregat, E., Fitoussi, C. and Bourdon, B.: A new method for TIMS high precision analysis of Ba and Sr isotopes for cosmochemical studies, J. Anal. At. Spectrom., 32(7), 1388–1399, https://doi.org/10.1039/C7JA00012J, 2017.

Zachos, J., Pagani, M., Sloan, L., Thomas, E. and Billups, K.: Trends, rhythms, and aberrations in global climate 65 Ma to present, Science, 292(5517), 686–693, 2001.

Zhang, L., Tang Wilson H., Zhang Lulu, and Zheng Jianguo: Reducing Uncertainty of Prediction from Empirical Correlations, Journal of Geotechnical and Geoenvironmental Engineering, 130(5), 526–534, https://doi.org/10.1061/(ASCE)1090-0241(2004)130:5(526), 2004.